

1 Integrated Geophysical Analysis of Rangpur Saddle: Insights on Tectonics and 2 Magnetic Mineral Potential of North-Western Bangladesh

3
4 Mohammad Tawhidur Rahman Tushar¹, Asif Ashraf², Md. Mahfuz Alam¹, Md Nasif Jamil¹, Saba Karim¹,
5 Md. Shahjahan³, Md. Anwar Hossain Bhuiyan¹

6
7 ¹Department of Geology, University of Dhaka, Dhaka-1000, Bangladesh

8 ²Department of Earth Sciences, University of Oregon, Eugene, Oregon-97401, United States of America

9 ³Geological survey of Bangladesh, 153 Pioneer Road, Dhaka-1000, Bangladesh

10
11 Correspondence to: Mohammad Tawhidur Rahman Tushar (mtrt@du.ac.bd) and Asif Ashraf (aashraf@uoregon.edu)

13 Abstract

14
15 The northwestern region of Bangladesh holds untapped potential for magnetic mineral deposits at
16 shallow depths. Unlike much of Bangladesh, characterized by thick sediments of the Bengal Basin,
17 this area is an extension of the Indian Shield, often referred to as the Stable Platform. It is also
18 geologically distinct, hosting structures related to the breakup of Pangea. The geology and
19 tectonics of this region have remained largely understudied. To address this gap, this study
20 integrates gravity, magnetic, seismic, and drilling data to investigate the subsurface structure and
21 evaluate the resource potential of the area. We utilize advanced filtering and modeling techniques,
22 including tilt derivatives and horizontal gradient methods, to understand the tectonic framework
23 and geometry of the subsurface structures. Our spatial analysis, using multiple geophysical
24 datasets, reveals dipolar magnetic anomalies, which we attribute to gabbroic intrusions along
25 extensional faults that define the region's horst and graben structures. To validate our
26 interpretations, we developed an integrated 2-D subsurface model that aligns with the observed
27 geophysical data. However, the study is limited by the availability of high-resolution seismic data
28 and the sparse distribution of drilling locations, which may affect the precision of our subsurface
29 characterization. Our findings provide crucial insights into the tectonic evolution of the stable
30 platform and underscore the economic potential of the Rangpur Saddle, the shallowest part of the
31 stable platform, for mineral exploration. These insights pave the way for further exploration and
32 development initiatives focused on uncovering the mineral wealth of this underexplored region.

34 1. Introduction

35
36 The northwestern part of Bangladesh is rich in potential mineral resources. The geological
37 diversity of this area suggests the presence of other valuable minerals that remain largely
38 unexplored (Akhtar, 2005; Hasan et al., 2023; Moon, 2022). In this area, basement rocks are
39 present at relatively shallow depths of 128 meters, hosting a spectrum of economic mineral
40 resources, including coal, limestone, white clay, and hard rock (Khan and Rahman, 1992).
41 Notably, Pirganj in the Rangpur district (**Figure 1**) records the country's highest magnetic
42 anomaly, suggesting the potential for magnetic mineral ore deposits. In the 1990s, drilling
43 activities were conducted in the region after developing a 2D subsurface model by the Geological
44 Survey of Bangladesh (GSB) in collaboration with the United States Geological Survey (USGS).
45 Despite these efforts, no noteworthy ore body was identified during the drilling process (Rahman

Deleted: distinct

Deleted: characterized by alternating magnetic highs and
lows...

Deleted: discernible

Deleted: &

51 ~~and Ullah, 2009). Moreover, the tectonic evolution of the Paleo-Proterozoic basement in the~~
52 ~~northwest region of the Bengal Basin still needs to be studied.~~

Deleted: &

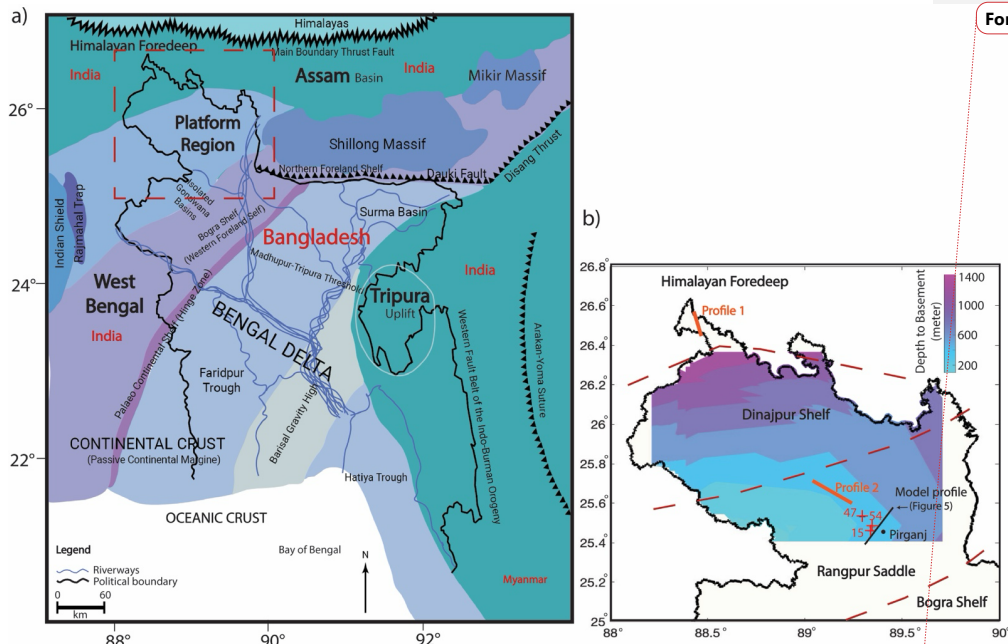
53
54 The study area is located in a region commonly referred to as the Rangpur platform or saddle
55 (Masum et al., 2021), an eastern extension of the Indian Shield (Alam et al., 2003). The northern
56 part of the Rangpur Saddle rests on a shallow Precambrian basement, ranging from 130 to 1000
57 meters in depth. This area of Bangladesh is geologically stable, characterized predominantly by
58 horsts and grabens, which were formed during the Cretaceous rifting of the Indian plate from the
59 Antarctica-Australia section of Gondwanaland (Curry, 1991; Curry ~~and Moore, 1974~~). Although
60 the basement primarily consists of diorite, tonalite, and granodiorite, it is also intersected by
61 pegmatite and mafic/ultramafic dykes (Hossain et al., 2007; Kabir et al., 2001).

Deleted: &

62
63 In this study, we explore the possibility of mafic dykes as the source of high magnetic anomalies
64 using multiple geophysical datasets while establishing the regional geological structure of this
65 significantly understudied area. We aim to conduct integrated spatial analysis and develop
66 subsurface models with gravity, magnetic, seismic, and drilling data to understand the regional
67 geological features. Gravity and magnetic data are widely used to understand and characterize
68 geological formations, particularly for identifying thin magnetic layers or faults (Adebiyi et al.,
69 2023; Jaffal et al., 2010). High-resolution potential field data help identify structures related to
70 local-scale mineralization that are covered by shallow alluvium or other unconsolidated sediments
71 (Hendrickson, 2016; McCafferty et al., 2014). Since potential field data can yield multiple
72 solutions (Filina et al., 2019), ~~we~~ also incorporate seismic and drilling data to constrain the
73 subsurface framework and produce more reliable results (Sundararajan, 2012). Our study applies
74 various filters to magnetic and gravity data to enhance and delineate regional crustal structures,
75 with a focus on highlighting structure edges where metallic mineral deposits are likely to be found
76 (Hildenbrand, 2000).

Deleted: . We

77



Formatted: English (US)

81 ▲
 82 Figure 1: (a) Regional geological map of Bangladesh adopted from Hossain et al. (2019), illustrating various
 83 geological and tectonic zones with distinct color coding. The names of neighboring countries are labeled in red. The
 84 red dashed box indicates the study area in the northwestern part of Bangladesh. (b) The map of the northwestern
 85 Bangladesh region shows basement depth with its tectonic subdivisions. Regional basement depths are collected from
 86 GSB and constructed from various seismic reflection surveys. Red dashed lines mark the approximate boundaries of
 87 the tectonic divisions. Seismic profiles (orange lines) and drilling locations (red plus signs) utilized in this study are
 88 also highlighted. Our specific study area, Pirganj, is also shown on the map, where the highest magnetic anomaly is
 89 observed. The integrated 2-D modeling profile of this study is also shown in this map with a solid black line.

90
 91 **2. Geological setting**

92
 93 Bangladesh, though geographically compact, possesses a complex and diverse geological
 94 framework shaped largely by its position within the Bengal Basin (Roy and Chatterjee, 2015). This
 95 region is primarily divided into two major tectonic units (Morgan and McIntire, 1959). To the
 96 northwest of the hinge zone (see **Figure 1a** for location), the stable platform region features a
 97 shallow basement composed predominantly of Precambrian-aged rocks (Uddin and Lundberg,
 98 1998). Conversely, the southeastern portion of the Bengal Basin comprises a geosynclinal basin,
 99 distinguished by significant sediment accumulation, with sediment thicknesses exceeding 12
 100 kilometers (Alam, 1989). This tectonic configuration highlights the geological contrasts between
 101 the stable platform and the more dynamic, subsiding basin to the southeast.

102
 103 The Bengal Basin, encompassing Bangladesh and parts of the neighboring Indian states of West
 104 Bengal, Assam, and Tripura, is situated at the northeastern edge of the Indian craton. It is one of

Deleted: McIntire

106 South Asia's largest peripheral collisional foreland basins, with a sedimentary sequence spanning
107 from the Early Cretaceous to the Holocene (DeCelles, 2011). The study area, located in the
108 northwest part of the basin and known as the stable platform, consists of three geological
109 components (Hossain et al., 2019): the Dinajpur Shelf, Rangpur Saddle, and the Bogra Shelf
110 (Figure 1b). The Himalayan Foredeep region, located just north of the Dinajpur Shelf, contains
111 the deepest basement in the stable platform (Figure 1b) and hosts numerous faults associated with
112 extensional tectonics (Figure 2a). South of the Foredeep region, the Dinajpur Shelf gently slopes
113 northward toward the Himalayan Foredeep at an angle of 1-3 degrees and is covered by recent
114 sedimentary deposits. The Rangpur Saddle, the southern block of the Dinajpur Shelf, connects the
115 Indian Shield to the Shillong Plateau and contains the shallowest basement in the Bengal Basin
116 (Jain et al., 2020) (Figure 1b). The Bogra Shelf, on the southern slope of the Rangpur Saddle, was
117 formed during the Early Cretaceous rifting of the Indian plate from Gondwana (Alam, 1989; Alam
118 et al., 2003). Both the Rangpur Saddle and Bogra Shelf host several horsts and graben, and half-
119 graben basins (Figure 2b).

Deleted: is

121 The entire northwestern Bangladesh is geologically stable with minimal folding impact that can
122 be traced back to Rodinia and Nuna or Columbia supercontinents (Ameen et al., 2007; Zhang et
123 al., 2012). Ameen et al. (2007) suggest that the basement is a separate micro-continental fragment
124 trapped during the northward migration of the Indian Plate, while Hossain et al. (2007) propose
125 that it is a continuation of the central Indian tectonic zone. During the Precambrian, only the stable
126 shelf of the Bengal basin was part of the Indian Plate within Gondwana. By the Middle Jurassic
127 (~170–175 Ma), the Indian Plate began drifting and became isolated by the end of the Paleocene
128 (~55.9 Ma) (Hossain et al., 2019). During the Late Paleozoic–Mid Mesozoic, the stable shelf was
129 developed as an intra-cratonic rift basin with Gondwana sediments in graben structures, followed
130 by Kerguelen igneous activity and widespread Rajmahal Trap volcanism (Hossain et al., 2019;
131 Valdiya, 2016).

Deleted: north-eastern

Deleted: from

Deleted: Luna

Deleted: Colombia

Deleted: ,

Deleted: becoming

133 The basement in our study area is the shallowest part of the Stable Shelf, which is uplifted to a
134 depth of 128 m from the surface, overlain by the Plio-Pleistocene Dupi Tila Sandstone and
135 Madhupur Clay, and is mainly composed of crystalline rocks, including granite, granodiorite, and
136 gneiss (Alam et al., 2003; Hossain et al., 2007). There is no outcrop of Precambrian basement in
137 this area, and the commonly observed horst and graben structures control the stratigraphic
138 subdivision. The Precambrian basement in this region lies beneath thick Cenozoic clastic deposits
139 and is primarily felsic in composition, intersected by mafic-ultramafic and occasional felsic dykes
140 (Chowdhury et al., 2022). Fault-bound graben basins within the basement contain Carboniferous
141 rock units from the Permian Period (286 to 245 million years ago) called the Gondwana formation,
142 marking the oldest sedimentary rocks in Bangladesh (Alam et al., 2003; Jain et al., 2020). Above
143 the Permian Gondwana formation is the Jurassic Rajmahal Trap Formation, consisting of volcanic
144 basalt strata (Alam, 1989; Roy and Chatterjee, 2015). The Shibganj Trapwash Formation overlays
145 it, formed through weathering and erosion of the underlying igneous rocks (Khan, 1991).

Deleted: (Rahman 1987),

147 The Rangpur Saddle serves as the subsurface extension of the Indian shield, stretching between
148 the Shillong Plateau to the east and the Rajmahal Hills to the west. Geophysical studies have
149 identified two major faults framing the Garo-Rajmahal gap: the Dhubri-Jamuna Fault (western
150 edge of Garo Hills) and the Rajmahal Fault (eastern edge of Rajmahal Hills), which encloses the
151 Rangpur saddle (Hossain et al., 2019). Tectonic activities, particularly extensional tectonics during

Deleted:)

161 continental rifting, have significantly disrupted the basement topography, forming numerous
 162 horsts and grabens (Ahamed et al., 2020; Khan and Rahman, 1992). Despite this, the study area
 163 remains predominantly flat with sediment covers (Khan, 1991) from the Pleistocene to the
 164 Holocene period (Reimann and Hiller, 1993). Near the Rangpur Saddle, the eastern part of the
 165 Indian Shield includes three major tectonic domains: Singhbhum Craton, Singhbhum Mobile Belt,
 166 and Chhotanagpur Gneissic Complex (Mukhopadhyay and Matin, 2020). Singhbhum Craton is
 167 characterized by prolonged crustal evolution during the Archean, comprising lithologies such as
 168 granitoids and metamorphic rocks. Singhbhum Mobile Belt underwent accretion and modification
 169 through volcanics, dyke swarms, and various intrusive bodies in the Proterozoic. Chhotanagpur
 170 Gneissic Complex comprises mainly of gneisses, amphibolites, and granulites with mafic dyke
 171 swarms, forming a structurally complex mobile belt. The tectonics of this region can be
 172 characterized by intra-cratonic structural depressions between the uplifted tectonic blocks. Seismic
 173 reflection studies indicate that the Moho in this region is complex and laminated, suggesting a
 174 history of tectonic and magmatic activity (Valdiya, 2016). In the West Bengal basin, the Moho is
 175 relatively shallow and horizontal (at a depth of 36 km), while other nearby regions (e.g., Kutch
 176 basin) have a dipping Moho influenced by tectonic processes (Rangin and Sibuet, 2017).

Deleted: &

177
 178 Magnetic minerals, particularly iron ore, are widely found across the Indian Shield. These iron
 179 deposits typically appear as metamorphosed banded iron or silica formations. In eastern India, the
 180 Precambrian iron ore of the Singhbhum-North Orissa region is a horseshoe-shaped synclinorium
 181 that contains the most significant iron deposits near Bangladesh. The first discovery of iron ore in
 182 Bangladesh is located on the Dinajpur slope of the Rangpur platform (Alam et al., 2003). Around
 183 30 km southwest of our study area, Masum et al. (2021) report iron ore-bearing basement rock
 184 about 30 km southwest of our study area, with the iron ores occurring as a thin, metamorphosed
 185 laminated layer.

Deleted: comprised

186
 187 To understand the geological succession in Pirganj and its surroundings, we present a generalized
 188 lithological depiction using data from EDH-15 and GDH-54 drill holes (Table 1).

189
 190 Table 1: Stratigraphic Succession of Pirganj and its adjoining Areas according to drill holes EDH-15 and GDH-54
 191

Deleted: &

| Age | Rock Units | Lithology | Thickness (m) |
|---------------------------------|------------|---|---------------|
| Recent | Alluvium | Loose sand, medium to coarse-grained | 52 |
| Unconformity | | | |
| Pliocene | Dupitila | Sandstone (SST), silty SST, pebbly SST, pebbly bed; SST: medium to coarse-grained, pebbles: quartzite, gneiss <u>and</u> schist | 33 |
| Unconformity | | | |
| Late Oligocene to Early Miocene | Surma | Alteration of SST and shales and their combination, sand and silty shale. SST: fine to medium-grained; shale: soft and sticky | 125 |
| Unconformity | | | |

Deleted: &

| | | | |
|------------------------------|------------------|---|----------------------|
| Late Cretaceous to Paleocene | Cherra Sandstone | Sandstone: medium to coarse-grained | 50 |
| Unconformity | | | |
| | Basement | Gabbro; Diorite, quartz diorite, granodiorite, quartz monazite. | 180+ (base not seen) |

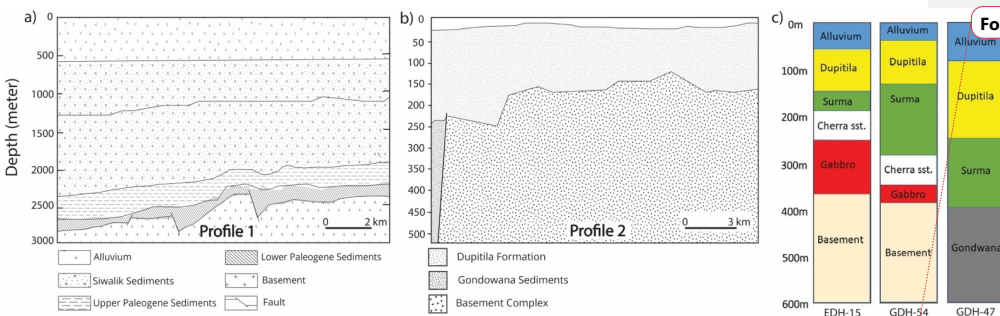


Figure 2: Interpretation of seismic and drilling data used for integrated geophysical analysis in this study. (a) and (b) present interpretations of the two seismic profiles analyzed. (c) shows the drilling log data, which correlates with the 2D subsurface models and assists in spatial analysis. Refer to Figure 1b for their locations. Seismic profile 1 is from Himalayan Foredeep region while profile 2 represents Rangpur Saddle. All the drilling logs are situated near the highest observed magnetic anomaly in Pirganj, located in Northwestern Bangladesh.

3. Data and Methodology

3.1 Geophysical Data

In this study, we apply an integrative analytical approach utilizing multiple geophysical datasets for spatial analysis and 2-D subsurface modeling. Our primary datasets are potential field data, specifically gravity and magnetic data, provided by the Geological Survey of Bangladesh (GSB). We use Bouguer gravity data and total magnetic intensity data for our analysis.

The gravity data presented in the paper were acquired through a land-based gravity survey conducted during the dry season (November–April) in the 1970s across approximately 8,000 km² in northwestern Bangladesh. Observation points were spaced 1–1.5 km apart, with elevations measured using digital leveling referenced to benchmarks from the Survey of Bangladesh. The Sylhet Gravity Base Station, connected to the IGSN 71 network, served as the national reference, and local sub-bases were established to correct for instrument drift. Two gravimeters were used—the analog Sodin Worden and the digital CG-5 AutoGrav with integrated GPS—with frequent cross-verification to ensure data accuracy. Standard geophysical corrections, including those for instrumental drift, tidal and latitude variations, and elevation differences, were applied, with Bouguer corrections calculated using a slab density of 2.0 g/cm³.

Formatted: English (US)

Deleted: Seismic

Deleted: Topography

227 Between 1979 and 1980, Hunting Geology & Geophysics Ltd. completed a nationwide
228 aeromagnetic survey for the Government of Bangladesh, under the auspices of the Geological
229 Survey of Bangladesh and Petrobangla. Flying a Geometrics G-803 proton magnetometer just 500
230 ft (≈ 152 m) above ground, the crew collected total-field data along flight lines oriented N 45° W
231 on a nominal 3 km grid (locally tightened to 1 km) and crossed them with tie-lines oriented N 45°
232 E at 5 km spacing. Measurements were recorded every two seconds with a resolution of ± 0.05 nT,
233 within a regional field that varied from 44 848 nT to 47 086 nT (inclinations $28^\circ 30'$ – $38^\circ 30'$,
234 declinations 13° W– 37° W). All readings were archived in both digital and analogue form, and the
235 data were uniformly shifted upward by 900 nT so that every value is positive.

236
237 The topography data used in our geophysical modelling (Figure S1) are obtained from the online
238 repository of the Scripps Institution of Oceanography, which are derived from satellite altimetry
239 (Smith and Sandwell, 1997). Additionally, we incorporate interpretations of seismic images
240 obtained from GSB to correlate our findings from gravity and magnetic data. However, raw
241 seismic images are unavailable, as private entities originally collected them. To further refine our
242 2-D integrated modeling, we use drilling data from three boreholes near our study area, also
243 provided by GSB (see Figure 1b for the locations).

244 245 **3.2 Methods**

246
247 For geophysical spatial analysis, we use gravity and magnetic anomaly maps. The Bouguer gravity
248 data from GSB are corrected for elevation. For the total magnetic intensity map, we apply a
249 differential reduction to the pole (RTP) to adjust the magnetic grid (Arkani-Hamed, 2007). This
250 correction involves computing magnetic inclination, declination, and total magnetic field values
251 based on the International Geomagnetic Reference Field (Alken et al., 2021) with a magnetic epoch
252 of 1980.

253
254 The next step in our spatial analysis methodology involves removing the regional trend from both
255 the gravity and magnetic data. This process, known as regional-residual separation, is essential for
256 isolating local anomalies by filtering out the broader, long-wavelength trends associated with
257 large-scale geological structures (Ashraf and Filina, 2023b; Kheyrollahi et al., 2021; Núñez-
258 Demarco et al., 2023). Total magnetic intensity anomalies arise from the combined effect of
259 induced and remanent magnetization in rocks. Induced magnetization is caused by the Earth's
260 ambient field acting on magnetic minerals, so it is aligned parallel to the present field, whereas
261 remanent magnetization is a permanent magnetization inherent to the rocks (acquired in the past)
262 that often points in a different direction (reflecting the Earth's field at the time of rock formation).
263 The total magnetization is the vector sum of the induced and remanent contributions. As a result,
264 the direction and relative magnitude of each component strongly influence the observed anomaly.
265 If the induced and remanent magnetization vectors are aligned, they reinforce each other to
266 produce a stronger (high-amplitude) anomaly; if they are opposed or significantly misaligned, they
267 partially cancel or reorient the net magnetization, which can weaken the anomaly or even yield
268 one of opposite polarity compared to what an induced-only model would predict. This interplay
269 complicates data interpretation, since assuming all magnetization is induced (parallel to today's
270 field) can lead to errors in locating or characterizing sources.

271
272 By removing these regional trends, we enhance the visibility of smaller-scale or high-frequency
273 anomalies, allowing subtle features and variations in the subsurface to be highlighted more

Deleted: modeling

275 effectively. To remove regional anomalies, we apply an upward continuation of 1000 m to the
276 Bouguer gravity data (**Figure 3a**). This approach simulates measuring the gravity field at a higher
277 elevation—1000 m in our case—effectively smoothing out high-frequency anomalies associated
278 with shallow or near-surface geological features (Balogun et al., 2023). For RTP magnetic
279 anomaly, we use a Gaussian filter to calculate the regional trend (**Figure 3b**). This Gaussian filter
280 acts as a low-pass filter, smoothing out high-frequency components in the dataset. After extracting
281 the regional anomaly from the potential field, we subtract it from the unfiltered total anomaly,
282 yielding the residual anomaly (**Figure 3**).

283
284 We apply several filters to the residual potential field data to enhance specific features and improve
285 interpretability (**Figure 3**). Under the framework of Poisson's theorem in potential-field theory,
286 taking a vertical derivative of gravity and performing a reduction-to-the-pole on magnetic data are
287 mathematically analogous operations and are equivalent Fourier-domain operations: both sharpen
288 source-edge contrasts while suppressing deep, long-wavelength signals, thus yielding mutually
289 consistent structural imagery (Blakely, 1996). The filters we have used involve various forms of
290 derivative operations, which help to highlight changes in the data that correspond to geological
291 boundaries, faults, or other structural details (Ibraheem et al., 2023; Ma et al., 2016; Nasuti et al.,
292 2019; Núñez-Demarco et al., 2023). For the residual RTP magnetic data, we apply and show two
293 filters: the horizontal derivative and the tilt derivative. The horizontal derivative filter, applied in
294 x-direction (i.e., across the longitudes) and y-direction (i.e., across the latitudes), accentuates
295 lateral changes in the magnetic field, helping to reveal abrupt variations. The tilt derivative filter,
296 however, is especially effective as an edge detector. It operates by combining both vertical and
297 horizontal gradients, effectively highlighting the edges of anomalous bodies. The tilt derivative
298 produces values that tend toward zero over magnetically flat regions, positive over rising areas,
299 and negative over falling areas, creating a clear demarcation of the edges of magnetic sources. As
300 a result, this filter enhances the boundaries of anomalies and helps pinpoint the locations and
301 shapes of features with minimal distortion across varying depths (Ashraf and Filina, 2023b; Pham
302 and Oliveira, 2023). We apply the lineament mapping techniques to map major structural
303 boundaries from the filtered magnetic data (Ashraf and Filina, 2023a, 2023b; Ogah and Abubakar,
304 2024; Zhang et al., 2024). Our approach focused on identifying gaps between magnetic stripes,
305 changes in the stripe orientation, and a significant reduction in stripe width. We also calculate the
306 analytical signals of the magnetic anomalies to highlight the areas with high magnetizing
307 amplitude (Nabighian, 1972; Roest and Pilkington, 1993) that may illuminate magnetic mineral
308 deposits (Mohamed et al., 2022). To calculate the analytical signal of the residual magnetic data,
309 we first compute the horizontal and vertical derivatives of the magnetic field in the x, y, and z
310 directions. The analytical signal was then derived by taking the square root of the sum of the
311 squares of these derivatives, yielding a map that represents the amplitude of the magnetic field
312 independent of direction and highlights the edges of magnetic sources. To validate our
313 interpretations, we cross-reference the magnetic lineaments with gravity data. Before validating
314 with gravity data, we filter the residual gravity data by applying the first vertical derivative and tilt
315 derivative to map major tectonic structures and delineate their boundaries.

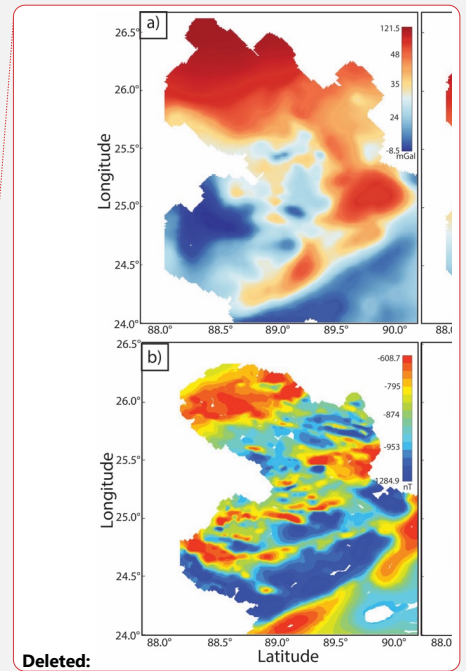
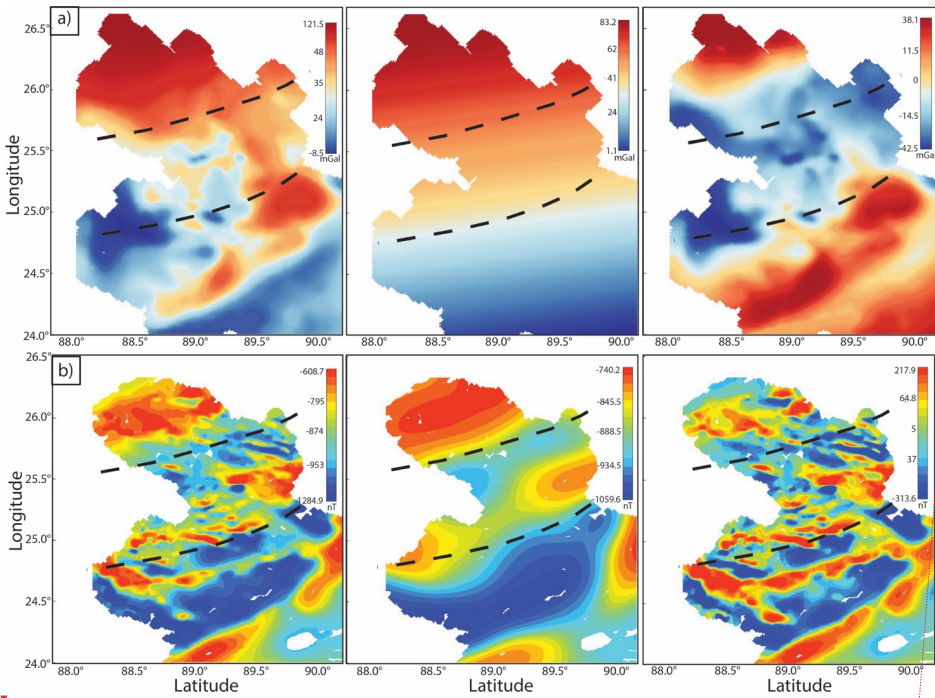
316
317 We also develop 2-D integrated models of the subsurface to examine the variations in the physical
318 properties of the rocks (density and magnetic susceptibility). We build our models using the GM-
319 SYS module within the Geosoft software suite, employing a 2-D approximation (Geosoft, 2021).
320 The GM-SYS model is extended to +/- 30000 km (i.e., infinity) along the X-axis and 90 km along

Deleted: These filters

Deleted: &

Deleted: &

324 the Z-axis to eliminate edge effects. By integrating gravity and magnetic data within this 2D
 325 context, we can delineate major geological boundaries and assess regional structural trends with
 326 sufficient accuracy for our research objectives. Our goal is to develop a simple subsurface structure
 327 that satisfactorily aligns with gravity, magnetic, and logging data without introducing excessive
 328 complexity that might overfit the potential field anomaly. Instead, we aim to replicate the general
 329 pattern of the observed anomaly in our 2D modeling, seeking to generate computed anomalies
 330 with comparable amplitude, wavelength, and phase to those observed in the potential fields.
 331



332
 333
 334 Figure 3: Potential field data maps of northwestern Bangladesh used in this study to analyze geological and tectonic
 335 features. (a) Gravity anomaly maps: from left to right, the Bouguer gravity anomaly, regional Bouguer gravity anomaly
 336 with 1000 m upward continuation, and residual Bouguer gravity anomaly. (b) Magnetic anomaly maps: from left to
 337 right, the RTP total magnetic anomaly, regional magnetic anomaly after Gaussian filtering, and residual magnetic
 338 anomaly. The black dashed lines show the boundary of Rangpur Saddle.

339
 340 **4. Result**

341
 342 **4.1 Integrated spatial analysis**

343
 344 In this study, we first establish the regional tectonic structures of northwestern Bangladesh through
 345 spatial analysis of multiple geophysical datasets. We utilize gravity, magnetic, seismic image

347 interpretations, and drilling log data to characterize the tectonic setup of this region. Our analysis
348 of residual magnetic and gravity anomalies reveals that the Rangpur Saddle exhibits distinctly
349 different geophysical characteristics compared to its northern counterpart, the Himalayan Foredeep
350 region. These differences are discernible in the long-wavelength or broad-scale geophysical
351 signatures across the two regions.

Deleted: distinct

352
353 In the Himalayan Foredeep, north of 26°N latitude, we observe a high residual Bouguer gravity
354 anomaly, ranging from approximately 5 to 30 mGal. In contrast, the Rangpur Saddle, located south
355 of this latitude, is marked by a low residual Bouguer gravity anomaly, typically between -22 and
356 0 mGal. Similarly, the Rangpur Saddle shows lower residual RTP total magnetic anomalies,
357 ranging from 0 to 260 nT compared to mostly high magnetic anomalies in north (~ 0 to 215 nT).
358 The spatial patterns of these anomalies also differ across the regions. South of 26°N latitude, in
359 the Rangpur Saddle, the horizontal and tilt derivative magnetic anomalies show a predominance
360 of NW-SE trending magnetic lineaments. North of this latitude, in the Himalayan Foredeep, the
361 magnetic anomaly trend shifts predominantly to a SW-NE orientation. Additionally, in the vertical
362 and tilt derivatives of the gravity data, we observe the most pronounced high gravity linear
363 anomaly patch trends NW-SE south of 26°N latitude, consistent with the magnetic anomaly trend
364 in this area. South of 26°30'N latitude, we see another linear high-gravity patch in the filtered
365 Bouguer gravity data trending NW-SE, indicating a different orientation than the other high-
366 gravity patch of the Rangpur Saddle region. These two high-gravity patches are also traceable in
367 the filtered magnetic anomalies, following the magnetic lineament mapping procedure. Notably,
368 some areas exhibit strong inverse gravity and magnetic field trends, where high gravity coincides
369 with low magnetic anomalies, or vice versa. One might expect a corresponding increase in the
370 gravity signal due to the higher density of the gabbroic intrusions relative to the overlying rocks;
371 however, this expected gravity anomaly is not observed in our data. We believe this discrepancy
372 arises from two interconnected factors. First, gravity and magnetic methods are most sensitive to
373 lateral variations in subsurface properties, and in our study area, the subsurface structures are
374 predominantly flat-lying. At depth, the gabbroic intrusions are laterally adjacent to felsic basement
375 rocks, and while the density contrast between these lithologies is modest (~0.1 g/cm³), their
376 magnetic susceptibilities differ significantly. This contrast produces a strong magnetic response
377 but only a subtle gravity anomaly that may be indistinguishable from background variations. Also,
378 the intrusions occur in fault-bounded graben fill that causes a localized low density (due to thick
379 low-density Gondwana sediments in the graben). Second, the spatial resolution of our gravity
380 survey, with a station spacing of approximately 3 km, is relatively coarse compared to the scale of
381 the gabbroic intrusions. As a result, any high-frequency gravity signals associated with these
382 smaller or more localized bodies are likely undersampled and thus not adequately captured in the
383 final gravity dataset. In brief, the high gravity areas correspond to uplifted blocks of dense
384 basement, whereas the magnetic highs occur on the flanks where intrusions have come up along
385 faults and the graben is filled with lighter sediment, yielding a relative gravity low.

Deleted: In

Deleted: -

Formatted: English (US)

Formatted: English (US)

386
387 Within the Rangpur Saddle region, we observe multiple oval dipolar patterns. From the RTP
388 residual magnetic anomaly data, we identify seven distinct patterns. The identification of these
389 patterns follows several consistent criteria. First, the dipolar magnetic anomalies are generally
390 oriented in a north-south direction. Second, each pattern features a magnetic high in the northern
391 section and a corresponding low to the south. Third, within each pattern, the size, area, and
392 amplitude of the magnetic high and low anomalies are comparable, contributing to a symmetrical

Deleted: semi-circular

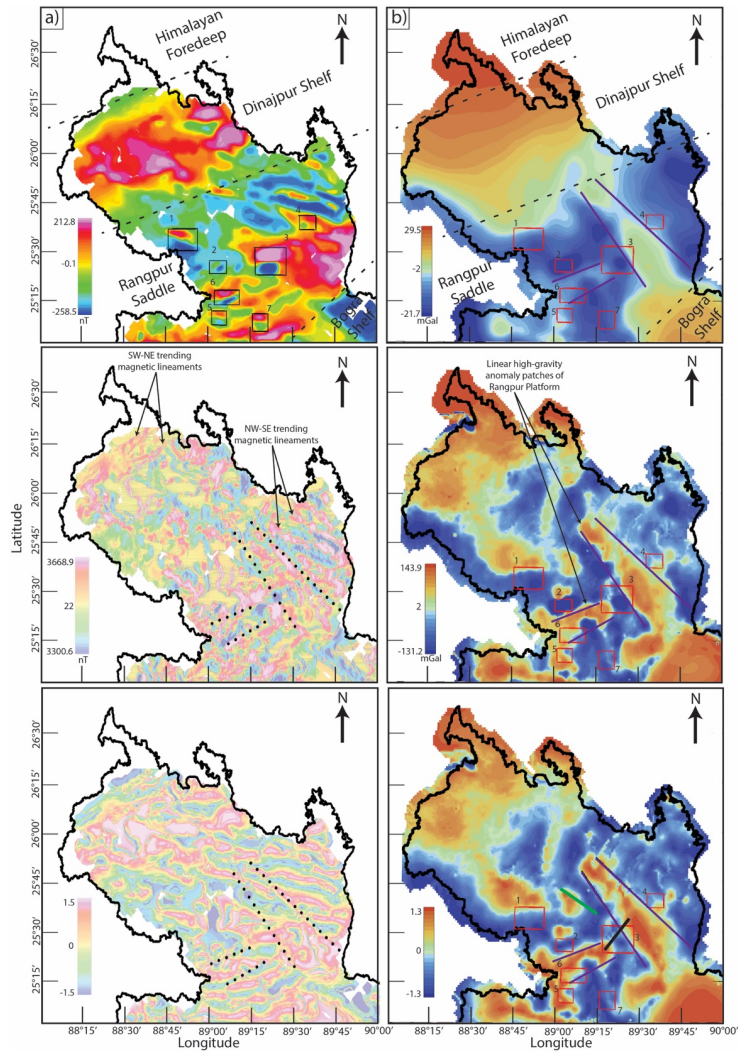
Deleted: characterized by alternating magnetic highs and lows...

Deleted: alternating high and low

400 structure. The filtered magnetic data also reveals possible signatures of remanently magnetized
401 sources, some of which may be reversely magnetized. At the Earth's magnetic field inclination of
402 approximately 45° in northwestern Bangladesh (based on the IGRF 1980 epoch used for RTP
403 correction), reversely magnetized sources such as gabbroic intrusions formed during past
404 geomagnetic reversals produce negative anomalies after RTP where positive anomalies would
405 align with the current field. Mapping these magnetic patterns onto the filtered gravity maps reveals
406 that they consistently lie near the boundary between high and low gravity anomalies. While most
407 of these magnetic patterns (patterns 1, 4, 5, 6, and 7) intersect only one boundary, a few patterns
408 (specifically patterns 2 and 3) touch boundaries on both sides.
409

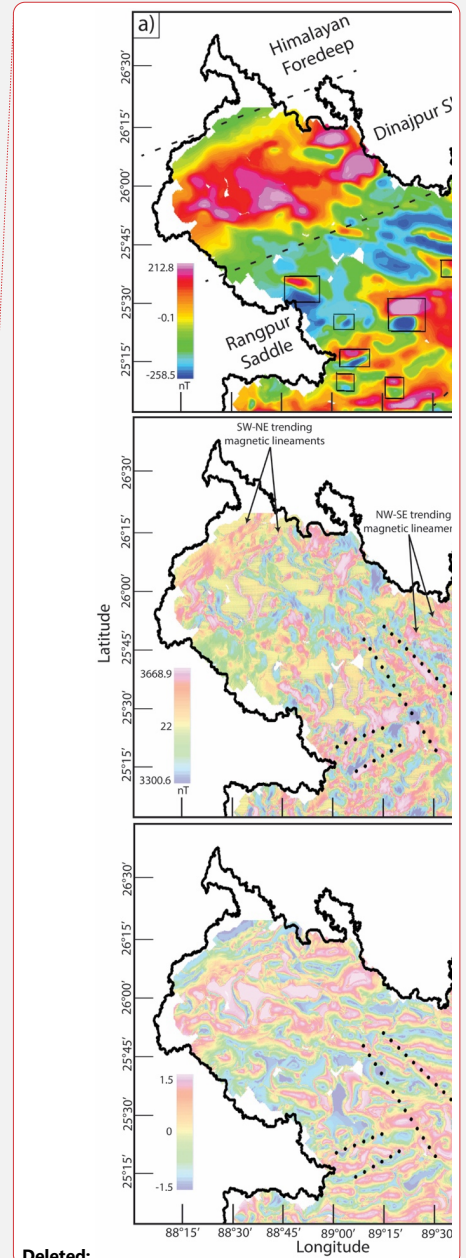
Deleted: Mapping these magnetic patterns of alternating highs and lows...

Formatted: English (US)



412

413 Figure 4: a) Magnetic anomaly maps of northwestern Bangladesh. The top panel displays the residual RTP total
 414 magnetic anomaly, the middle panel shows the first horizontal derivative in the x-direction (across longitudes), and
 415 the bottom panel illustrates the tilt derivative. Black boxes highlight areas where oval dipolar magnetic patterns are
 416 observed. Dotted black lines in the middle and bottom panels indicate boundaries of high gravity regions. b) Bouguer
 417 gravity anomaly maps of northwestern Bangladesh. The top panel presents the residual Bouguer gravity anomaly, the
 418 middle panel shows the first vertical derivative, and the bottom panel displays the tilt derivative. High gravity regions
 419 are outlined by purple solid lines, and red boxes indicate areas with dipolar magnetic patterns. The solid green line in



Deleted:

Deleted: semi-circular...oval dipolar magnetic patterns of alternating highs and lows ...re observed. Dotted black lines in the middle and bottom panels indicate boundaries of high gravity regions. b) Bouguer gravity anomaly maps of northwestern Bangladesh. The top panel presents the residual Bouguer gravity anomaly, the middle panel shows the first vertical derivative, and the bottom panel displays the tilt derivative. High gravity regions are outlined by purple solid lines, and red boxes indicate areas with dipolar magnetic patterns of alternating highs and lows

[1]

435 the bottom panel represents seismic profile 2 from Figure 2. The thick solid black line shows the 2-D integrated
436 modelling profile of Figure 5.

437 **4.2 Integrated subsurface modeling**

438

439 We develop a 2-D subsurface model utilizing gravity, magnetic, and drilling log data (**Figure 5**).
440 The goal of this model is to approximate the observed anomalies on a local scale while aligning
441 with the available drilling log information (**Figure 2c**). The magnetic anomaly modeled in Figure
442 5 is the residual RTP anomaly, reflecting local high-frequency features after removing regional
443 trends. Importantly, we do not aim to achieve a precise fit between the observed data and calculated
444 anomalies. This decision is driven by the fact that the observed potential field data are influenced
445 by regional structures, and without sufficient seismic information, constructing a reliable regional
446 model is not feasible. Instead, we focus on developing a simplified version of the subsurface model
447 that reasonably fits the observed anomalies and drilling data.

448

449 To ground the 2-D model in reality, we incorporated available drilling log information (**Figure 2**).
450 Based on these logs, the model includes five sedimentary layers above a crystalline basement. The
451 shallowest layer is assigned as alluvium, extending to a depth of 50 meters or less. Beneath the
452 alluvium, we sequentially include the Dupitila, Surma, and Cherra sandstone layers. The variable
453 thickness of these sedimentary layers comes from the drilling log information, except for the
454 Gondwana layer. The thickness of Gondwana is approximated based on the gravity fit. Below
455 these layers, we model a mafic intrusion of gabbro, which occurs within fault structures that have
456 developed within the underlying felsic basement.

457

458 The resulting model indicates that a horst and graben structure is the most plausible configuration
459 when considering the regional geological context. This structural interpretation also provides a
460 reasonable match to the observed geophysical anomalies. Additionally, based on information from
461 drilling log GDH 47, we assign a layer of Gondwana sediments within the graben basin, which is
462 contributing to the low observed gravity in this region.

463

464 Densities in the model are derived from drilling data, reflecting the unique lithological
465 characteristics of each unit. To get an initial guess on the density, we developed a gravity model
466 for profile 1 that has seismic-derived subsurface information (Figure S2). The alluvium, Dupitila,
467 Surma, and Cherra Sandstone layers are modeled with densities of 2000, 2200, 2500, and 2670
468 g/cm³, capturing their progressive compaction and mineral composition. The Gondwana unit,
469 enriched with coal deposits, exhibits a notably lower density of 2200 g/cm³, consistent with its
470 organic-rich composition. Beneath these layers, the felsic basement and gabbroic intrusion stand
471 out with densities of 2800 and 3000 g/cm³, highlighting their denser crystalline structure and mafic
472 origins.

473

474 Between 400 and 800 meters depth, the gabbroic intrusion begins to follow the fault plane. The
475 thickness of both the Gondwana layer and the underlying felsic basement is determined from the
476 amplitude of the calculated gravity and magnetic anomalies. The thickness of the Gondwana layer
477 influences the minimum value of the calculated gravity anomaly, while the amplitude of the
478 magnetic anomaly helps determine the depth of the gabbroic intrusion. Notably, our calculated
479 anomalies are of high frequency. This occurs because our modeling does not incorporate all
480 regional structures; instead, it focuses only on local structures. As a result, the calculated anomalies
481 reflect primarily local or high-frequency potential field anomalies.

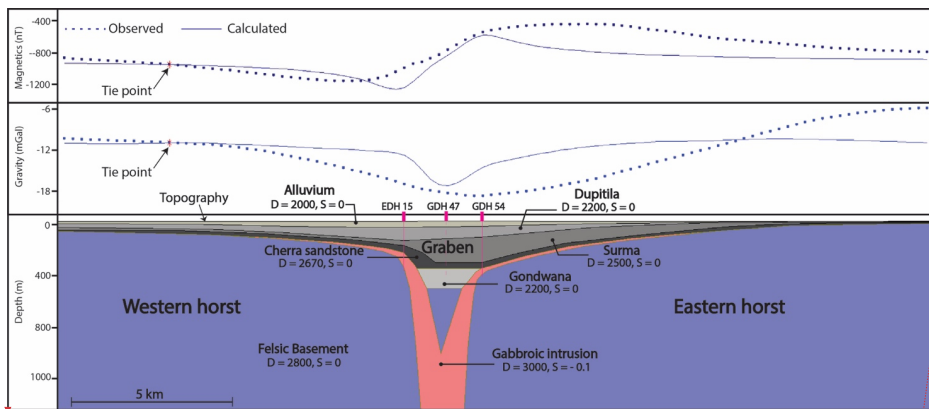
Deleted: ¶

Formatted: English (US)

Formatted: English (US)

483
484
485
486
487
488
489
490

Our 2D subsurface model reveals two horst structures with a graben basin in the middle. We refer to these as the eastern and western horsts based on their geographic locations. In the model, the western horst structure is depicted as deeper, consistent with the observed gravity anomaly, which shows lower gravity in the western horst compared to the eastern horst. Our model does not include the broader horst structure on the eastern side, which likely explains the discrepancy between the calculated and observed anomalies over the eastern horst.



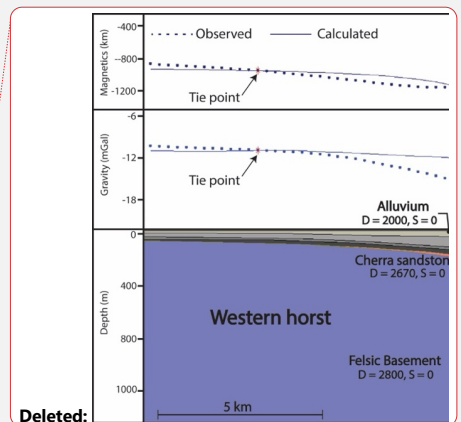
491

Figure 5: Integrated 2D geophysical model over the highest magnetic anomaly in northwestern Bangladesh. See Figure 1b and 4c for the location of the model profile. The top panel presents the total magnetic intensity anomaly, and the middle panel shows the gravity anomaly, with observed (dotted) and calculated (solid) data. Tie points, marked by red stars, indicate where the calculated anomalies are vertically shifted to align with the observed data. The bottom panel illustrates the subsurface model, with geological units represented by distinct colors. 'D' denotes density (g/cm^3), and 'S' denotes magnetic susceptibility (SI units). Bold pink vertical dashes mark the locations of drilling logs used to constrain subsurface units. Thin vertical pink lines extend downward from these surface locations. Solid pink lines beneath EDH 15 and GDH 54 indicate where the forward model is directly tied to lithological boundaries from well logs. In contrast, the dashed pink line beneath GDH 47 reflects an interpretative connection, as this well does not lie directly along the modeling profile.

492
493
494
495
496
497
498
499
500
501
502
503
504
505
506
507
508
509
510
511
512
513
514
515
516

We acknowledge the mismatch between the observed and calculated anomalies in our forward model. We aim to adopt the simplest model that captures the essential features of the observed anomaly without introducing unnecessary complexity. While even basic 2-D models can yield multiple valid solutions, incorporating intricate structures without strong geological constraints would increase interpretive ambiguity. Additionally, our model is inherently two-dimensional and thus cannot fully represent the three-dimensional geological variations present in the study area, such as the broad, shallow eastern horst, whose lateral extent likely contributes to higher observed gravity values. Finally, our modeling profile spans a smaller area than the full potential field survey (refer to section 3.1), resulting in calculated anomalies that emphasize localized, high-frequency features, whereas the observed data reflect broader, lower-frequency trends. Our forward model is calculated on 250 m spacing, whereas the gravity data were acquired every 1–1.5 km and the magnetic data every 5 km.

Deleted: larger



Deleted:

Deleted: The red

Deleted: show

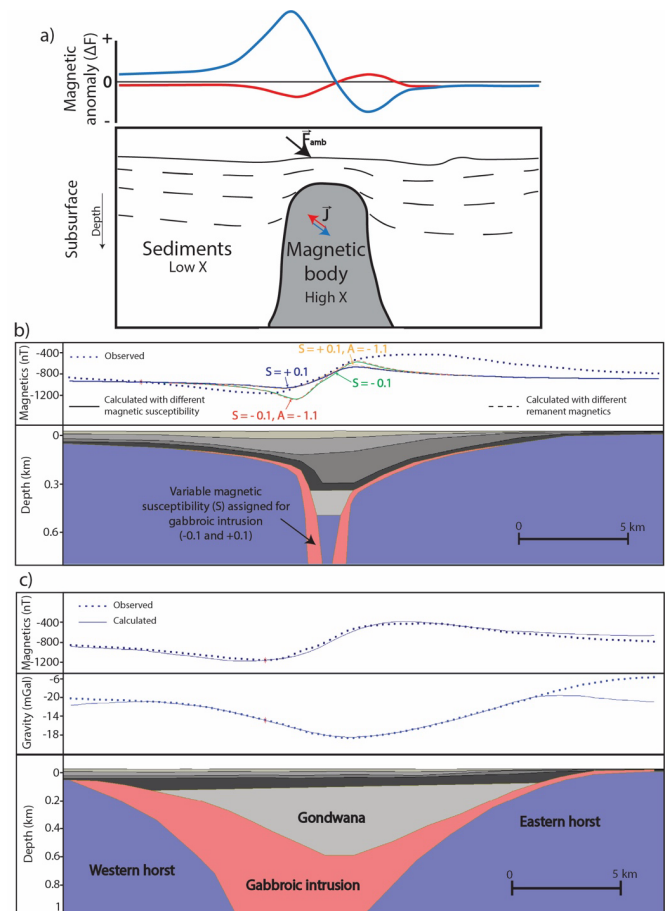
Deleted: location

Deleted: the

Deleted: the

524 Furthermore, we also test alternative models, which further support that the presented version
525 offers the most concise and geologically reasonable solution. First, we test how the polarization
526 direction of the remanent magnetization affects the total magnetic intensity reading of a dome-
527 shaped magnetic body (Figure 6a). We incorporate both remanent magnetization (A) and
528 magnetic susceptibility (S) in the forward model affects the total magnetic intensity and its polarity
529 (Figure 6b). When we assign a positive susceptibility contrast ($S = +0.1$ SI), the calculated
530 anomaly captures the general shape of the observed data more accurately in terms of slope, but the
531 amplitude (highs and lows) is notably lower than the observed values. In contrast, using a negative
532 susceptibility yields calculated amplitudes that closely match the observed highs and lows;
533 however, the overall shape shows a poorer fit, with significant mismatches in the slopes. Because
534 of the better match for the amplitudes, we prefer the negative susceptibility for the magnetic body
535 in our forward model. We also implemented an additional component of remanent magnetization
536 (A) to the magnetic body, fixed at -1.1 A/m, and tested combinations such as $S = -0.1$ SI with A
537 $= -0.1$ A/m and $S = +0.1$ SI with $A = -1.1$ A/m. These combinations yielded a similar response,
538 primarily increasing the amplitude of the anomaly without changing the overall trend. In
539 conclusion, while the additional remanent magnetization component amplifies the anomaly
540 magnitude, it does not significantly affect the trend or alter the interpretation of the model. We
541 have also developed a model that shows a perfect fit between the observed and calculated anomaly
542 (Figure 6c). However, to achieve that, we need to completely abandon the constraints from well-
543 logs and regional structural context based on gravity and magnetic data. For these reasons, we
544 adopt a simplified, geologically grounded model that balances interpretive clarity with structural
545 realism.

546



547
548
549
550
551
552
553
554
555
556
557
558
559
560
561

Figure 6: a) Conceptual illustration showing polarization direction of the remanent magnetization affecting the total magnetic intensity reading of a dome-shaped magnetic body. The synthetic total-field anomaly (ΔF) profiles are calculated for a concealed high-susceptibility intrusion beneath low-susceptibility sediments. The blue curve represents the response when magnetization is purely induced parallel to the present-day ambient field F_{amb} , producing a simple positive-negative (dipolar) signature. The red curve shows how the anomaly shape and amplitude are modified when an oblique remanent magnetization component J is added to the induced vector. b) Investigation on how incorporating both remanent magnetization (A) and magnetic susceptibility (S) in the forward model affects the total magnetic intensity and its polarity. c) 2-D forward modelling along the same profile as Figure 5, where we have achieved a perfect fit between the calculated and observed anomalies except for the model edges.

Formatted: Font: 12 pt

562 **5. Discussion**

563

564 **5.1 Basement structure**

565

566 One of the primary goals of this paper is to understand the basement structure and tectonic setup
567 of the Rangpur Saddle. Our findings reveal significant differences in the basement structures of
568 the Rangpur Saddle compared to its northern counterparts, evident in both gravity and magnetic
569 data. A key distinction is the depth to basement between these regions (**Figure 1b**). Previous
570 studies consistently suggest that the basement depth in the Rangpur Saddle is shallower than in the
571 Dinajpur Shelf. However, those studies were based on limited seismic and drilling data. Our
572 results, however, indicate a more complex basement geometry than previously understood.
573 Filtered gravity and seismic data presented here suggest that the Rangpur Saddle region contains
574 both shallow and deep basement features (**Figure 4b**). Considering regional tectonics, we propose
575 that high gravity values correspond to shallow horst structures, while low gravity values indicate
576 deeper graben structures. However, the frequency of horsts and grabens is significantly lower in
577 the Rangpur Saddle compared to the northern Himalayan Foredeep and the Dinajpur Shelf (**Figure**
578 **2a and 2b**). In the Rangpur region, we identified only two horsts of notable width and length. The
579 boundaries of these horst structures also appear as lineaments in the filtered magnetic data (**Figure**
580 **4a**), suggesting the presence of major structural boundaries.

581

582 Furthermore, differences in the directions of magnetic lineaments between the Rangpur Saddle
583 region and its northern counterparts—the Dinajpur Shelf and the Himalayan Foredeep—suggest
584 variations in paleo-tectonic stress orientation (**Figure 4a, 7a and 7b**). Existing literature
585 characterizes northwestern Bangladesh predominantly with extensional tectonics (Gani and Alam,
586 2003). Near the Himalayan Foredeep boundary, SW-NE trending magnetic lineaments indicate a
587 paleo-principal stress direction oriented NW-SE. Moving southward into the Dinajpur Shelf, NW-
588 SE trending magnetic lineaments become more common (**Figure 7b**), pointing to a shift in the
589 principal stress direction associated with extensional tectonics. In the Rangpur Saddle, these NW-
590 SE trending lineaments are even more frequent, especially in the eastern part, indicating a greater
591 intensity of paleo-tectonic stress in this region compared to the Dinajpur Shelf. Based on traced
592 magnetic and gravity lineaments, the stable platform can be divided into four distinct zones
593 (**Figure 7d**). In Zone 1, located in the northern part, lineaments predominantly trend SW-NE, with
594 only a few exceptions. Moving southward into Zone 2, there is a mixture of two differently
595 trending lineaments: SW-NE and NW-SE. In Zone 3, in the easternmost section of the stable
596 platform, lineaments primarily trend NW-SE, aligning with the eastern horst. Finally, in Zone 4,
597 the southernmost region, lineaments generally follow an SW-NE trend, corresponding with the
598 western horst. This subdivision highlights the complex nature of past tectonic processes in this
599 region.

600

601 We also identify seven **oval dipolar** patterns of magnetic highs and lows. When mapped onto
602 gravity data, these patterns consistently align with the boundaries between high and low gravity
603 patches, indicating the **possible** boundaries between horsts and grabens. Drilling log data near the
604 most prominent magnetic anomaly reveals the presence of gabbro, which may explain these
605 **dipolar** magnetic **patterns**. Furthermore, these regions of **dipolar** magnetic patterns also spatially
606 correlate with overall high magnetization (**Figure 7a**). We propose that these gabbro formations

Deleted: &

Deleted: 6a & 6b

Deleted: Royhan

Deleted: Mustafa

Deleted: 6b

Deleted: 6d

Deleted: semi-circular

Deleted: alternating

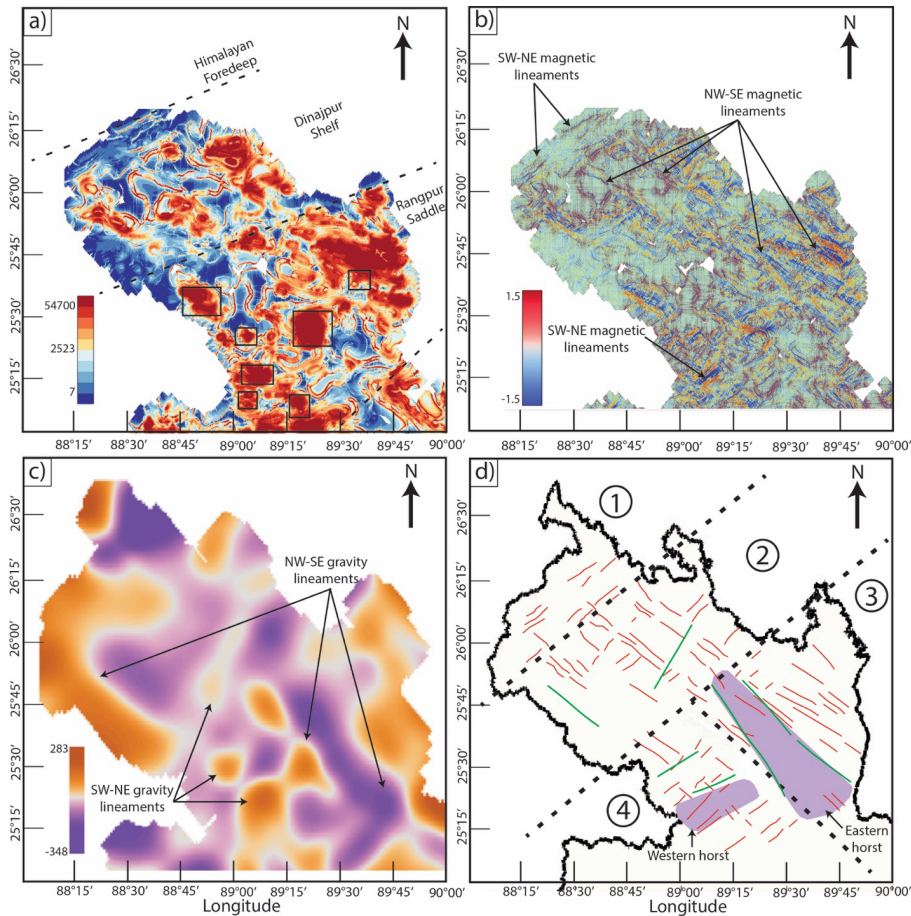
Deleted: alternating

Deleted: highs and lows

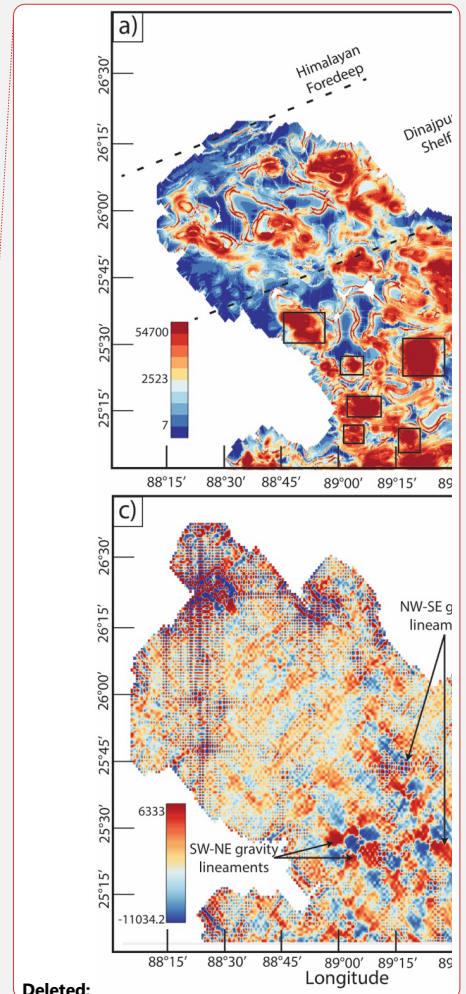
Deleted: alternating

Deleted: 6a

619 resulted from intrusions along normal faults, formed by extensional tectonics, which define the
 620 boundaries between horsts and grabens.
 621



622
 623 **Figure 7:** Filtered potential field maps of the northwestern stable platform region of Bangladesh, highlighting major
 624 tectonic structures and boundaries. (a) Analytical signal map derived from the magnetic anomaly (methodology
 625 detailed in Sect. 3), showing magnetization amplitudes across the region. Black boxes indicate areas of **oval dipolar**
 626 magnetic patterns, as shown in Figure 4a. Dashed lines represent boundaries between established tectonic
 627 subdivisions. (b) Total horizontal gradient map of the magnetic anomaly, calculated by applying a first horizontal
 628 derivative filter in the X-direction, followed by a first horizontal derivative filter in the Y-direction. (c) Total horizontal
 629 derivative (similar method as in 'b') of the residual gravity anomaly. This map is developed after applying upward
 630 continuation to the residual gravity data to a level where high-resolution artifacts are no longer present in the derivative
 631 map. (d) Map displaying traced magnetic lineaments (in red) from 'b' and gravity lineaments (in green) from 'c'.
 632 Black dashed lines indicate regional subdivisions based on mapped tectonic lineaments. Purple polygons mark horst
 633 structures in the Rangpur Saddle, interpreted from filtered gravity data (refer to Figure 4b).



- Deleted:**
- Deleted:** 6
- Deleted:** semi-circular
- Deleted:** with alternating highs and lows
- Deleted:** of the residual gravity anomaly.

639
640
641
642
643
644
645
646
647
648
649
650
651
652
653
654
655
656
657
658
659
660
661
662
663
664
665
666
667
668
669
670
671
672
673
674
675
676
677
678
679
680
681
682
683

5.2 Economic mineral potential

Our integrated spatial analysis and 2-D modeling reveal that the Rangpur Saddle contains at least two prominent horst and graben structures. The 2-D model results (Figure 5), supported by drilling log data, confirm the presence of gabbroic bodies along normal faults within these structures. This suggests that the most prominent oval-shaped dipolar magnetic signature has strong potential to host iron-bearing rocks such as gabbro. When the other similar patterns are mapped onto the gravity data, they consistently correspond to the boundaries between high and low gravity zones, marking the transitions between horsts and grabens. We interpret these gabbroic intrusions as products of magmatic emplacement along extensional faults (Figure 8), consistent with processes associated with the early stages of continental rifting. Furthermore, analysis of lineament orientations (Figure 7d) indicates that, except in the western horst region, most of the interpreted magmatic emplacement appears to be controlled by NW–SE oriented lineaments.

The breakup process involved rifting events that progressively separated the Indian subcontinent from the other Gondwanaland constituents (Veevers, 2004). The breakup of Gondwanaland involved multiple rifting episodes and magmatic activities. While the Central Atlantic Magmatic Province (CAMP) exemplifies rift-related magmatism during the Triassic-Jurassic breakup of Pangea, the Rangpur Saddle's tectonic evolution is more directly tied to the Cretaceous rifting of the Indian plate from Antarctica-Australia (Curry, 1991; Hossain et al., 2019). This rifting facilitated extensional faulting and mafic intrusions, analogous to processes observed in CAMP but occurring later in the Mesozoic. In such tectonic settings, normal faulting and rift-related subsidence create pathways for mafic magmas to ascend (Brune et al., 2023; Pirajno and Santosh, 2014; Ruppel, 1995), leading to the emplacement of gabbroic and other mafic intrusions within the crust (Magee et al., 2019).

Mafic magma intrusions are commonly observed along extensional fault planes in tectonically active regions worldwide. Troll et al. (2021) shows that in NW Scotland, Long Loch Fault acted as dynamic magma conduit with its movements facilitating the ascent of ultrabasic magmas. These magmas intruded along faults and fractures, leading to the destabilization and collapse of existing cumulate layers, forming extensive breccias. A study on Mesozoic gabbroic intrusions in the High Atlas Mountains highlights their emplacement along extensional faults during the rifting associated with the Central Atlantic Magmatic Province, where more than 50% of gabbro samples exhibit stable magnetization from magnetite which is identified as the primary component (Calvin et al., 2017). Fuller and Waters (1929) have extensively studied horsts and graben structures in southern Oregon where they found emplacement of volcanic and intrusive rocks are closely associated with extensional faulting. These normal faults and the resulting grabens provide pathways for magma to ascend and intrude, which is evident from the prevalence of rhyolitic, dacitic, and andesitic vents as well as basaltic dikes aligned with the faults.

Mafic intrusions along fault zones are often associated with magnetic mineral deposits, which can be economically significant as ore bodies (Zhou et al., 2005). For instance, magnetite deposits are found within mafic intrusions along the fault planes in Egypt, which exhibit high magnetic anomalies, facilitating their detection and delineation (Kharbish et al., 2022; Mousa et al., 2020).

- Deleted:** indicate
- Deleted:** hosts
- Deleted:** significant
- Deleted:** modeling
- Deleted:** , corroborated
- Deleted:** the
- Deleted:** (Figure 7). We propose
- Deleted:** result from
- Deleted:** ,
- Deleted:** typically observed during
- Deleted:** breakup.

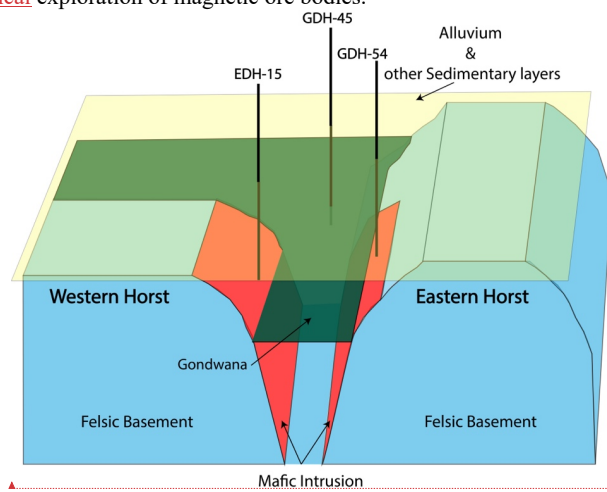
Deleted: Key rifting episodes and magmatic activities, such as the formation of the Central Atlantic Magmatic Province and related tectonic movements, facilitated this separation (Thompson et al., 2019; Veevers, 2004).

Formatted: English (US)

Deleted: &

700 Also, in Central Iran, iron-bearing magnetic mineral deposits are observed to exhibit high magnetic
701 and gravity anomalies (Kheyrollahi et al., 2021).

702
703 Based on current geochemistry data, the Rangpur Saddle holds significant potential for magnetic
704 mineral ore deposits, driven by its mafic-ultramafic sequences and iron-rich dykes (Ameen et al.,
705 2021). High Fe₂O₃ content in hornblendites and associated minerals like magnetite and ilmenite
706 indicate strong magnetization. The tectonic setting, with extensive magmatic intrusions, provides
707 ideal conditions for mineralization. These findings highlight the region as a possible target for
708 future geophysical exploration of magnetic ore bodies.



709
710
711 Figure 8: 3D schematic diagram illustrating the tectonic structures in Pirganj, where the highest magnetic anomaly is
712 observed in Bangladesh. The felsic basement, depicted in blue blocks, includes two horsts, as shown in Figure 5d.
713 Possible mafic intrusions along the faults are indicated in red. Sedimentary layers are represented by a single horizontal
714 layer in specific colors, with the graben basin likely filled with Gondwana sediments shown in green, and other
715 sedimentary layers, including alluvium, shown in yellow, which also represents the topography of the region. The
716 approximate locations of the three drilling logs used in this study (refer to Figure 1b for their locations) are also
717 indicated.

718 5.3 Limitations and Future Research

719
720 Compared to other regions globally, limited published research exists for our study area, restricting
721 our ability to draw on established models and findings. Situated at the eastern edge of the Indian
722 Shield, this area transitions into a different tectonic subdivision, creating a tectonic complexity
723 that cannot be fully resolved with the available low-resolution data. The scarcity of high-resolution
724 datasets, such as regional-scale seismic surveys, further limits our capacity to delineate regional
725 structures accurately. Currently, no regional or localized high-resolution datasets from ground-
726 based surveys are widely available, though such data could enhance future studies. Additionally,
727 the available well log data are predominantly shallow, reaching depths of approximately 500
728 meters, which limits insights into deeper geological and tectonic features beyond 2 kilometers.
729 Petrographic descriptions of the basement rocks are also rudimentary, as they are primarily based
730

Deleted: promising

Formatted: English (US)

Deleted: 7

Deleted: .

734 on a limited number of well logs, most of which were drilled before the 1990s, leaving significant
735 gaps in our understanding of the area's deeper subsurface geology.

737 Future research in this region will focus on constructing detailed three-dimensional (3D) models
738 of the subsurface to enhance our understanding of the geological framework. This will involve
739 compiling a comprehensive dataset repository that integrates historical seismic reflection data,
740 including those acquired by private entities. Given the shallow nature of the basement, which lies
741 between approximately 128 and 1000 meters depth, high-resolution gravity and magnetic data will
742 be critical for resolving fine-scale structural features. To achieve the necessary spatial resolution,
743 precision ground-based gravity and magnetic surveys are recommended. Specifically, we propose
744 a targeted geophysical survey in areas exhibiting oval-shaped dipolar magnetic anomalies, using
745 station spacing of 500 meters or less. Such high-density measurements will improve our ability to
746 detect and delineate narrow mafic intrusions at shallow depths. In addition, developing a regional
747 tomographic model using either local earthquake data or ambient seismic noise will provide
748 complementary constraints on subsurface structures and further refine interpretations of the
749 geological setting.

751 The study area is characterized by complex tectonic structures shaped by a diverse tectonic history.
752 While the current study has focused on the Rangpur Saddle, future research will expand to cover
753 the entire northwestern part of Bangladesh, including the Himalayan Foredeep and the Eocene
754 Hinge region, which represents a Palecontinental shelf. Such expanded coverage will provide
755 deeper insights into the tectonic evolution and geological complexity of the area.

757 Conclusion

758
759 This study provides a geophysical investigation of the northwestern region of Bangladesh,
760 revealing its significant potential for mineral resource exploration. The integration of gravity,
761 magnetic, seismic, and drilling data has allowed us to identify key tectonic features, such as
762 gabbroic intrusions along extensional faults, some which may host of valuable magnetic mineral
763 deposits. Despite the limitations in data resolution and coverage, our findings offer important
764 insights into the region's geological evolution and resource potential. Future work should prioritize
765 acquiring more detailed geophysical data and expanding drilling campaigns to refine the
766 understanding of subsurface structures and evaluate the feasibility of mineral extraction. The
767 Rangpur Saddle, as the shallowest part of the stable platform, emerges as a promising target for
768 future mineral exploration endeavors.

770 Data availability

771 All raw data can be provided by the corresponding authors upon request.

774 Author contribution

775
776 [▲] Muhammad Tawhidur Rahman Tushar was involved in conceptualization, methodology, software,
777 validation, formal analysis, investigation, resources, data curation, writing – original draft, writing
778 – review and editing, visualization. Asif Ashraf contributed to conceptualization, methodology,

Formatted: English (US)

Deleted: developing

Deleted: , providing a more detailed

Deleted: its

Deleted: structure

Deleted: effort

Deleted: include creating

Deleted: incorporates

Deleted: from

Deleted: depth

Deleted: region

Deleted: also

Deleted: essential

Deleted: a thorough analysis. This may require

Deleted: measurements through

Deleted: surveys to accurately collect

Deleted: .

Deleted: comprehensive

Deleted: suggest the presence

Formatted: Font: 14 pt

Formatted: Font: 12 pt, Not Bold

797 software, validation, formal analysis, investigation, resources, data curation, writing – original
798 draft, writing – review and editing, and visualization. Md. Mahfuz Alam worked on software
799 development, validation, and formal analysis. Md Nasif Jamil contributed to writing – review and
800 editing and visualization. Saba Karim was involved in writing – review and editing and
801 visualization. Md. Shahjahan contributed to conceptualization, investigation, resources, project
802 administration, and supervision. Md. Anwar Hossain Bhuiyan was involved in writing – review
803 and editing, project administration, supervision, and funding acquisition.

804

805 **Competing interests**

806

807 The authors declare that they have no conflict of interest.

808

809 **Acknowledgment**

810

811 The gravity, magnetic, and seismic data, along with drilling information used in this study, were
812 graciously provided by the Geological Survey of Bangladesh (GSB), and the authors deeply
813 appreciate their support and collaboration. The authors also thank Asef Jamil Ajwad for his
814 assistance with computational facilities during the research. Special acknowledgment is made for
815 the Oasis Montaj classroom subscription and for the use of Geosoft Oasis Montaj v8.4 for data
816 processing and modeling. Finally, gratitude is extended to the Department of Geology, University
817 of Dhaka, for providing access to essential infrastructure and resources.

818

819 **Financial support**

820

821 This work was funded by the National Science and Technology Fellowship, awarded by the
822 Ministry of Science and Technology, Bangladesh.

823

824 **References**

825

826 Adebisi, L. S., Eluwole, A. B., Fajana, A. O., Salawu, N. B., and Saleh, A.: Contrasting structures
827 of the Southern Benue trough and the contiguous crystalline basement as observed from high-
828 resolution aeromagnetic data, *Sci Rep*, 13, 21516, <https://doi.org/10.1038/s41598-023-48639-8>,
829 2023.

830 Ahamed, S., Hossain, D., and Alam, J.: Exploring Basement Surface relationship of north-west
831 Bengal Basin using satellite images and tectonic modeling,
832 <https://doi.org/10.48550/ARXIV.2004.02734>, 2020.

833 Akhtar, A.: Mineral resources and their economic significance in national development:
834 Bangladesh perspective, *SP*, 250, 127–134, <https://doi.org/10.1144/GSL.SP.2005.250.01.12>,
835 2005.

836 Alam, M.: Geology and depositional history of Cenozoic sediments of the Bengal Basin of
837 Bangladesh, *Palaeogeography, Palaeoclimatology, Palaeoecology*, 69, 125–139,
838 [https://doi.org/10.1016/0031-0182\(89\)90159-4](https://doi.org/10.1016/0031-0182(89)90159-4), 1989.

- 839 Alam, M., Alam, M. M., Curray, J. R., Chowdhury, M. L. R., and Gani, M. R.: An overview of
840 the sedimentary geology of the Bengal Basin in relation to the regional tectonic framework and
841 basin-fill history, *Sedimentary Geology*, 155, 179–208, [https://doi.org/10.1016/S0037-](https://doi.org/10.1016/S0037-0738(02)00180-X)
842 [0738\(02\)00180-X](https://doi.org/10.1016/S0037-0738(02)00180-X), 2003.
- 843 Alken, P., Thébault, E., Beggan, C. D., Amit, H., Aubert, J., Baerenzung, J., Bondar, T. N., Brown,
844 W. J., Califf, S., Chambodut, A., Chulliat, A., Cox, G. A., Finlay, C. C., Fournier, A., Gillet, N.,
845 Grayver, A., Hammer, M. D., Holschneider, M., Huder, L., Hulot, G., Jager, T., Kloss, C., Korte,
846 M., Kuang, W., Kuvshinov, A., Langlais, B., Léger, J.-M., Lesur, V., Livermore, P. W., Lowes, F.,
847 J., Macmillan, S., Magnes, W., Manda, M., Marsal, S., Matzka, J., Metman, M. C., Minami, T.,
848 Morschhauser, A., Mound, J. E., Nair, M., Nakano, S., Olsen, N., Pavón-Carrasco, F. J., Petrov,
849 V. G., Ropp, G., Rother, M., Sabaka, T. J., Sanchez, S., Saturnino, D., Schnepf, N. R., Shen, X.,
850 Stolle, C., Tangborn, A., Tøffner-Clausen, L., Toh, H., Torta, J. M., Varner, J., Vervelidou, F.,
851 Vigneron, P., Wardinski, I., Wicht, J., Woods, A., Yang, Y., Zeren, Z., and Zhou, B.: International
852 Geomagnetic Reference Field: the thirteenth generation, *Earth Planets Space*, 73, 49,
853 <https://doi.org/10.1186/s40623-020-01288-x>, 2021.
- 854 Ameen, S. M. M., Wilde, S. A., Kabir, Md. Z., Akon, E., Chowdhury, K. R., and Khan, Md. S. H.:
855 Paleoproterozoic granitoids in the basement of Bangladesh: A piece of the Indian shield or an
856 exotic fragment of the Gondwana jigsaw?, *Gondwana Research*, 12, 380–387,
857 <https://doi.org/10.1016/j.gr.2007.02.001>, 2007.
- 858 Ameen, S. M. M., Tapu, A.-T., and Hossain, M. S.: Precambrian Basement Rock of Bangladesh
859 and Its Metallic Minerals, in: *Bangladesh geosciences and resources potential*, CRC Press Books,
860 25–54, 2021.
- 861 ~~Arkani-Hamed, J.: Differential reduction to the pole: Revisited, *GEOPHYSICS*, 72, L13–L20,
862 <https://doi.org/10.1190/1.2399370>, 2007.~~
- 863 Ashraf, A. and Filina, I.: New 2.75-D gravity modeling reveals the low-density nature of
864 propagator wakes in the Juan de Fuca plate, *Tectonophysics*, 869, 230127,
865 <https://doi.org/10.1016/j.tecto.2023.230127>, 2023a.
- 866 Ashraf, A. and Filina, I.: Zones of Weakness Within the Juan de Fuca Plate Mapped From the
867 Integration of Multiple Geophysical Data and Their Relation to Observed Seismicity, *Geochem*
868 *Geophys Geosyst*, 24, e2023GC010943, <https://doi.org/10.1029/2023GC010943>, 2023b.
- 869 Balogun, O. B., Akereke, O. F., and Nwobodo, A. D.: Understanding the Constraints to the Correct
870 Application of the Upward Continuation Operation in Gravity Data Processing, *Pure Appl.*
871 *Geophys.*, 180, 3787–3811, <https://doi.org/10.1007/s00024-023-03348-1>, 2023.
- 872 ~~[Blakely, R. J.: *Potential theory in gravity and magnetic applications*, Cambridge university press,
873 1996.](#)~~
- 874 Brune, S., Kolawole, F., Olive, J.-A., Stamps, D. S., Buck, W. R., Buiter, S. J. H., Furman, T., and
875 Shillington, D. J.: Geodynamics of continental rift initiation and evolution, *Nat Rev Earth Environ*,
876 4, 235–253, <https://doi.org/10.1038/s43017-023-00391-3>, 2023.

Deleted: Anon: Geosoft, 2021.

- 878 Calvin, P., Ruiz-Martínez, V. C., Villalaín, J. J., Casas-Sainz, A. M., and Moussaid, B.:
879 Emplacement and Deformation of Mesozoic Gabbros of the High Atlas (Morocco):
880 Paleomagnetism and Magnetic Fabrics, *Tectonics*, 36, 3012–3037,
881 <https://doi.org/10.1002/2017TC004578>, 2017.
- 882 Chowdhury, K. R., Hossain, M. S., and Khan, M. S. H. (Eds.): *Bangladesh geosciences and*
883 *resources potential*, First edition., CRC Press, Boca Raton, 610 pp., 2022.
- 884 Curray, J. R.: Geological history of the Bengal geosyncline, *Journal of Association of Exploration*
885 *Geophysicists*, 12, 209–219, 1991.
- 886 Curray, J. R. and Moore, D. G.: Sedimentary and Tectonic Processes in the Bengal Deep-Sea Fan
887 and Geosyncline, in: *The Geology of Continental Margins*, edited by: Burk, C. A. and Drake, C.
888 L., Springer Berlin Heidelberg, Berlin, Heidelberg, 617–627, [https://doi.org/10.1007/978-3-662-](https://doi.org/10.1007/978-3-662-01141-6_45)
889 [01141-6_45](https://doi.org/10.1007/978-3-662-01141-6_45), 1974.
- 890 DeCelles, P. G.: Foreland Basin Systems Revisited: Variations in Response to Tectonic Settings,
891 in: *Tectonics of Sedimentary Basins*, edited by: Busby, C. and Azor, A., Wiley, 405–426,
892 <https://doi.org/10.1002/9781444347166.ch20>, 2011.
- 893 Filina, I., Biegert, E. K., Sander, L., Tschirhart, V., Bundalo, N., and Schiek-Stewart, C.: Integrated
894 imaging: A powerful but undervalued tool, *The Leading Edge*, 38, 720–724,
895 <https://doi.org/10.1190/tle38090720.1>, 2019.
- 896 Fuller, R. E. and Waters, A. C.: The Nature and Origin of the Horst and Graben Structure of
897 Southern Oregon, *The Journal of Geology*, 37, 204–238, 1929.
- 898 Hasan, M. M., Monir, A., and Hassan, M.: Evaluating the Energy and Mineral Resources Prospect
899 and Future Development in Bangladesh: A Review, <https://doi.org/10.2139/ssrn.4484598>, 2023.
- 900 Hendrickson, M. D.: Geologic interpretation of aeromagnetic and chemical data from the Oaks
901 Belt, Wabigoon subprovince, Minnesota: implications for Au-rich VMS deposit exploration, *Can.*
902 *J. Earth Sci.*, 53, 176–188, <https://doi.org/10.1139/cjes-2015-0141>, 2016.
- 903 Hildenbrand, T. G.: Regional Crustal Structures and Their Relationship to the Distribution of Ore
904 Deposits in the Western United States, Based on Magnetic and Gravity Data, *Economic Geology*,
905 95, 1583–1603, <https://doi.org/10.2113/95.8.1583>, 2000.
- 906 Hossain, I., Tsunogae, T., Rajesh, H. M., Chen, B., and Arakawa, Y.: Palaeoproterozoic U–Pb
907 SHRIMP zircon age from basement rocks in Bangladesh: A possible remnant of the Columbia
908 supercontinent, *Comptes Rendus Geoscience*, 339, 979–986,
909 <https://doi.org/10.1016/j.crte.2007.09.014>, 2007.
- 910 Hossain, Md. S., Khan, Md. S. H., Chowdhury, K. R., and Abdullah, R.: Synthesis of the Tectonic
911 and Structural Elements of the Bengal Basin and Its Surroundings, in: *Tectonics and Structural*
912 *Geology: Indian Context*, edited by: Mukherjee, S., Springer International Publishing, Cham, 135–
913 218, https://doi.org/10.1007/978-3-319-99341-6_6, 2019.

914 Ibraheem, I. M., Tezkan, B., Ghazala, H., and Othman, A. A.: A New Edge Enhancement Filter
915 for the Interpretation of Magnetic Field Data, *Pure Appl. Geophys.*, 180, 2223–2240,
916 <https://doi.org/10.1007/s00024-023-03249-3>, 2023.

917 Jaffal, M., Goumi, N. E., Kchikach, A., Aïfa, T., Khattach, D., and Manar, A.: Gravity and
918 magnetic investigations in the Haouz basin, Morocco. Interpretation and mining implications,
919 *Journal of African Earth Sciences*, 58, 331–340, <https://doi.org/10.1016/j.jafrearsci.2010.03.012>,
920 2010.

921 Jain, A. K., Banerjee, D. M., and Kale, V. S.: *Tectonics of the Indian Subcontinent*, Springer
922 International Publishing, Cham, <https://doi.org/10.1007/978-3-030-42845-7>, 2020.

923 Kabir, Z. M., Chowdhury, K. R., Akon, E., Kazi, A. I., and Ameen, S. M. M.: Petrogenetic Study
924 of Precambrian Basement Rocks from Maddhapara, Dinajpur, Bangladesh, *Bangladesh*
925 *Geoscience Journal*, 7, 1–18, 2001.

926 Khan, A. A. and Rahman, T.: An analysis of the gravity field and tectonic evaluation of the
927 northwestern part of Bangladesh, *Tectonophysics*, 206, 351–364, [https://doi.org/10.1016/0040-1951\(92\)90386-K](https://doi.org/10.1016/0040-1951(92)90386-K), 1992.

929 Khan, F. H.: *Geology of Bangladesh*, 1991.

930 Kharbish, S., Eldosouky, A. M., and Amer, O.: Integrating mineralogy, geochemistry and
931 aeromagnetic data for detecting Fe–Ti ore deposits bearing layered mafic intrusion, Akab El-
932 Negum, Eastern Desert, Egypt, *Sci Rep*, 12, 15474, <https://doi.org/10.1038/s41598-022-19760-x>,
933 2022.

934 Kheyrollahi, H., Alinia, F., and Ghods, A.: Regional magnetic and gravity structures and
935 distribution of mineral deposits in Central Iran: Implications for mineral exploration, *Journal of*
936 *Asian Earth Sciences*, 217, 104828, <https://doi.org/10.1016/j.jseas.2021.104828>, 2021.

937 Ma, G., Huang, D., and Liu, C.: Step-Edge Detection Filters for the Interpretation of Potential
938 Field Data, *Pure Appl. Geophys.*, 173, 795–803, <https://doi.org/10.1007/s00024-015-1053-6>,
939 2016.

940 Magee, C., Ernst, R. E., Muirhead, J., Phillips, T., and Jackson, C. A.: Magma transport pathways
941 in large igneous provinces: lessons from combining field observations and seismic reflection data,
942 in: *Dyke Swarms of the World: A Modern Perspective*, 45–85, 2019.

943 Masum, M., Hoque, M. N., Akbar, M. A., Mahmud, Z., Rana, M. S., Razzaque, M. A., and Amin,
944 M. A.: Geology and Precambrian Banded Iron Formation formed at Rangpur Platform in
945 Bangladesh, *International Journal Of Engineering Research And Development*, 17, 43–57, 2021.

946 McCafferty, A. E., Stoeser, D. B., and Van Gosen, B. S.: Geophysical interpretation of U, Th, and
947 rare earth element mineralization of the Bokan Mountain peralkaline granite complex, Prince of
948 Wales Island, southeast Alaska, *Interpretation*, 2, SJ47–SJ63, <https://doi.org/10.1190/INT-2014-0010.1>, 2014.

950 Mohamed, A., Abdelrady, M., Alshehri, F., Mohammed, M. A., and Abdelrady, A.: Detection of
951 Mineralization Zones Using Aeromagnetic Data, *Applied Sciences*, 12, 9078,
952 <https://doi.org/10.3390/app12189078>, 2022.

953 Moon, J. W.: *The Mineral Industry of Bangladesh*, U.S. Geological Survey, 2022.

954 Morgan, J. P. and McIntire, W. G.: [Quaternary Geology of The Bengal Basin, East Pakistan And
955 India](https://doi.org/10.1130/0016-7606(1959)70[319:QGOTBB]2.0.CO;2), *Geol Soc America Bull*, 70, 319, [https://doi.org/10.1130/0016-
956 7606\(1959\)70\[319:QGOTBB\]2.0.CO;2](https://doi.org/10.1130/0016-7606(1959)70[319:QGOTBB]2.0.CO;2), 1959.

957 Mousa, S. A. W., Abdel Nabi, S. H., Araffa, S. A. S., Mansour, S. A., and Al Deep, M. A. I.:
958 Geophysical exploration of titanomagnetite ore deposits by geomagnetic and geoelectric methods,
959 *SN Appl. Sci.*, 2, 444, <https://doi.org/10.1007/s42452-020-2206-5>, 2020.

960 [Mukhopadhyay, D. and Matin, A.: Recent Studies on the Singhbhum Craton, PINSA, 86,
961 https://doi.org/10.16943/ptinsa/2020/49788, 2020.](https://doi.org/10.16943/ptinsa/2020/49788)

962 [Nabighian, M. N.: The Analytic Signal of Two-Dimensional Magnetic Bodies With Polygonal
963 Cross-Section: Its Properties And Use For Automated Anomaly Interpretation, *Geophysics*, 37,
964 507–517, https://doi.org/10.1190/1.1440276, 1972.](https://doi.org/10.1190/1.1440276)

965 Nasuti, Y., Nasuti, A., and Moghadas, D.: STDR: A Novel Approach for Enhancing and Edge
966 Detection of Potential Field Data, *Pure Appl. Geophys.*, 176, 827–841,
967 <https://doi.org/10.1007/s00024-018-2016-5>, 2019.

968 Núñez-Demarco, P., Bonilla, A., Sánchez-Bettucci, L., and Prezzi, C.: Potential-Field Filters for
969 Gravity and Magnetic Interpretation: A Review, *Surv Geophys*, 44, 603–664,
970 <https://doi.org/10.1007/s10712-022-09752-x>, 2023.

971 Ogah, A. J. and Abubakar, F.: Solid mineral potential evaluation using integrated aeromagnetic
972 and aeroradiometric datasets, *Sci Rep*, 14, 1637, <https://doi.org/10.1038/s41598-024-52270-6>,
973 2024.

974 Pham, L. T. and Oliveira, S. P.: Edge Enhancement of Magnetic Sources Using the Tilt Angle and
975 Derivatives of Directional Analytic Signals, *Pure Appl. Geophys.*, 180, 4175–4189,
976 <https://doi.org/10.1007/s00024-023-03375-y>, 2023.

977 Pirajno, F. and Santosh, M.: Rifting, intraplate magmatism, mineral systems and mantle dynamics
978 in central-east Eurasia: An overview, *Ore Geology Reviews*, 63, 265–295,
979 <https://doi.org/10.1016/j.oregeorev.2014.05.014>, 2014.

980 Rahman, Md. M. and Ullah, S. E.: Inversion of Gravity Data for Imaging of a Sediment-basement
981 Interface: A Case Study in the Northwestern Part of Bangladesh, *Pure Appl. Geophys.*, 166, 2007–
982 2019, <https://doi.org/10.1007/s00024-009-0530-1>, 2009.

983 [Rangin, C. and Sibuet, J. C.: Structure of the northern Bay of Bengal offshore Bangladesh:
984 Evidences from new multi-channel seismic data, *Marine and Petroleum Geology*, 84, 64–75,
985 https://doi.org/10.1016/j.marpetgeo.2017.03.020, 2017.](https://doi.org/10.1016/j.marpetgeo.2017.03.020)

Deleted: and McINTIRE, W. G.: QUATERNARY GEOLOGY OF THE BENGAL BASIN, EAST PAKISTAN AND INDIA

Deleted: Nabighian, M. N.: THE ANALYTIC SIGNAL OF TWO-DIMENSIONAL MAGNETIC BODIES WITH POLYGONAL CROSS-SECTION: ITS PROPERTIES AND USE FOR AUTOMATED ANOMALY INTERPRETATION, GEOPHYSICS...

- 994 Reimann, K. U. and Hiller, K.: Geology of Bangladesh, 1993.
- 995 Roest, W. R. and Pilkington, M.: Identifying remanent magnetization effects in magnetic data,
996 GEOPHYSICS, 58, 653–659, <https://doi.org/10.1190/1.1443449>, 1993.
- 997 Roy, A. B. and Chatterjee, A.: Tectonic framework and evolutionary history of the Bengal Basin
998 in the Indian subcontinent, *Current Science*, 109, 271–279, 2015.
- 1000 **Gani, Royhan and Alam, Mustafa:** Sedimentation and basin-fill history of the Neogene clastic
1001 succession exposed in the southeastern fold belt of the Bengal Basin, Bangladesh: a high-
1002 resolution sequence stratigraphic approach, *Sedimentary Geology*, 155, 227–270,
[https://doi.org/10.1016/S0037-0738\(02\)00182-3](https://doi.org/10.1016/S0037-0738(02)00182-3), 2003.
- 1003 Ruppel, C.: Extensional processes in continental lithosphere, *J. Geophys. Res.*, 100, 24187–24215,
1004 <https://doi.org/10.1029/95JB02955>, 1995.
- 1005 Smith, W. H. F. and Sandwell, D. T.: Global Sea Floor Topography from Satellite Altimetry and
1006 Ship Depth Soundings, *Science*, 277, 1956–1962, <https://doi.org/10.1126/science.277.5334.1956>,
1007 1997.
- 1008 Sundararajan, N.: A General Perspective on Geophysical Methods in Mineral Exploration, in: On
1009 a Sustainable Future of the Earth's Natural Resources, 53–83, 2012.
- 1010 **Troll, V. R., Mattsson, T., Upton, B. G. J., Emeleus, C. H., Donaldson, C. H., Meyer, R., Weis, F.,**
1011 **Dahrén, B., and Heimdal, T. H.:** Fault-Controlled Magma Ascent Recorded in the Central Series
1012 of the Rum Layered Intrusion, NW Scotland, *Journal of Petrology*, 61, ega093,
1013 <https://doi.org/10.1093/ptrology/egaa093>, 2021.
- 1014 Uddin, A. and Lundberg, N.: Unroofing history of the eastern Himalaya and the Indo-Burman
1015 ranges; heavy-mineral study of Cenozoic sediments from the Bengal Basin, Bangladesh, *Journal*
1016 *of Sedimentary Research*, 68, 465–472, <https://doi.org/10.2110/jsr.68.465>, 1998.
- 1017 Valdiya, K. S.: *The Making of India*, Springer International Publishing, Cham,
1018 <https://doi.org/10.1007/978-3-319-25029-8>, 2016.
- 1019 Veevers, J. J.: Gondwanaland from 650–500 Ma assembly through 320 Ma merger in Pangea to
1020 185–100 Ma breakup: supercontinental tectonics via stratigraphy and radiometric dating, *Earth-*
1021 *Science Reviews*, 68, 1–132, <https://doi.org/10.1016/j.earscirev.2004.05.002>, 2004.
- 1022 Zhang, H., Greco, F., Sacek, V., Geng, M., and Liu, P.: Editorial: Applications of gravity
1023 anomalies in geophysics, *Front. Earth Sci.*, 12, 1349161,
1024 <https://doi.org/10.3389/feart.2024.1349161>, 2024.
- 1025 Zhang, S., Li, Z.-X., Evans, D. A. D., Wu, H., Li, H., and Dong, J.: Pre-Rodinia supercontinent
1026 Nuna shaping up: A global synthesis with new paleomagnetic results from North China, *Earth and*
1027 *Planetary Science Letters*, 353–354, 145–155, <https://doi.org/10.1016/j.epsl.2012.07.034>, 2012.

Deleted: Gani, M.

Deleted: Alam, M.:

Deleted: Thompson, J. O., Moulin, M., Aslanian, D., De
Clarens, P., and Guillocheau, F.: New starting point for the
Indian Ocean: Second phase of breakup for Gondwana,
Earth-Science Reviews, 191, 26–56,
<https://doi.org/10.1016/j.earscirev.2019.01.018>, 2019.†

1035 Zhou, M.-F., Robinson, P. T., Leshner, C. M., Keays, R. R., Zhang, C.-J., and Malpas, J.:
1036 Geochemistry, Petrogenesis and Metallogenesis of the Panzhihua Gabbroic Layered Intrusion and
1037 Associated Fe–Ti–V Oxide Deposits, Sichuan Province, SW China, *Journal of Petrology*, 46,
1038 2253–2280, <https://doi.org/10.1093/petrology/egi054>, 2005.

1039

Page 12: [1] Deleted

Asif Ashraf

7/20/25 12:41:00 PM

Page 12: [1] Deleted

Asif Ashraf

7/20/25 12:41:00 PM

Page 12: [1] Deleted

Asif Ashraf

7/20/25 12:41:00 PM